Langmuir and Langmuir–Blodgett Films of Amphiphilic Hexa-*peri*-hexabenzocoronene: New Phase Transitions and Electronic Properties Controlled by Pressure

Niels Reitzel,[a] Tue Hassenkam,[a] Konstantin Balashev,[a] Torben R. Jensen,[b] Paul B. Howes,[b] Kristian Kjaer,[b] Andreas Fechtenkötter,[c] Natalia Tchebotareva,[c] Shunji Ito,[c] Klaus Müllen,[c] and Thomas Bjørnholm*[a]

Abstract: We present the synthesis as well as the structural and electronic properties of an amphiphilic derivative of hexaalkylhexa-*peri*-hexabenzocoronene (HBC), which contains one alkyl substituent that is terminated with a carboxylic acid group. The molecules form well-defined Langmuir films when spread from a solution at the air–water interface. Grazing-incidence X-ray diffraction (GIXD) and X-ray reflectivity studies of the Langmuir monolayer reveal two crystallographic phases at room temperature which depend on the surface pressure applied to the film. Scattering from very well-ordered ($\xi =$ 200–400 Å) π-stacked lamellae of HBC molecules tilted $\approx 45^\circ$ relative to the surface normal is observed in the low-pressure phase. In this phase, the HBC molecules pack in a rectangular two-dimensional unit cell with $a = 22.95$ Å and $b = 4.94$ Å. In the high-pressure phase, coherence from the π stack is lost. This is a consequence of stress induced by the crystallization of the substituent alkyl chains into a hexagonal lattice, which has a trimerized superstructure in one direction: $a = 3 \times b =$ 15.78 Å, $b = 5.26$ Å, $\gamma = 120^\circ$, $A =$ 71.9 Å$^2 = 3 \times 23.9$ Å^2. Thin monolayer films can be transferred to solid supports by the Langmuir–Blodgett (LB) technique. Atomic force microscopy (AFM) with atomic resolution reveals the crystalline packing of alkyl chains in the high-pressure phase. Kelvin force microscopy (KFM) shows a clear potential difference between the high- and low-pressure phases. This is discussed in terms of orbital delocalization (band formation) in the highly coherent low-pressure phase, which is in contrast to the localized molecular orbitals present in the high-pressure phase. The highly coherent π stack is expected to sustain a very high charge-carrier mobility.

Keywords: Langmuir–Blodgett films · liquid crystals · pi interactions · self-assembly · structure elucidation

Introduction

Polycyclic aromatic hydrocarbons that spontaneously organize into mesogenic columnar materials with strong π–π interactions have recently attracted considerable attention owing to their rich and intriguing structural behavior and to their potential applications as vectorial transport layers in new organic devices.[1–8] The latter includes xerography, electrophotography, molecular electronics, and solar cells. Hexasubstituted hexa-*peri*-hexabenzocoronenes (HBCs) are particularly promising members of this family because they have shown unusually high charge-carrier mobilities along the π-stacked columns in the bulk mesogenic phases, both for the *n*-alkyl and for the phenylenealkyl derivatives.[8] Further functionalization of the alkyl sidegroups by the termination of one or all alkyl chains with a carboxylic acid group has recently been shown to allow complexation with polymeric cations and to provide new structures in which hydrogen bonding and π stacking compete as the main driving force for the organization of the bulk material.[9, 10] To further understand the organizational principles of these materials and to develop the possibilities of nanoscale manipulation and processing, we have investigated Langmuir[11] and Langmuir–Blodgett[12] (LB) films of the monoacid derivative of HBC (MAHBC; **1**) shown in Figure 1. As a general means of

[a] Prof. T. Bjørnholm, N. Reitzel, Dr. T. Hassenkam, Dr. K. Balashev
Nano-Science Center, Department of Chemistry
University of Copenhagen
Universitetsparken 5, 2100 Copenhagen (Denmark)
Fax: (+45) 35321810
E-mail: tb@nano.ku.dk

[b] T. R. Jensen, P. B. Howes, K. Kjaer
Condensed Matter Physics and Chemistry Department
Risø National Laboratory, 4000 Roskilde (Denmark)

[c] A. Fechtenkötter, N. Tchebotareva, S. Ito, Prof. K. Müllen
Max-Planck Institut für Polymerforschung
Ackermannweg 10, 55128 Mainz (Germany)

  0947-6539/01/0722-4894 $ 17.50+.50/0

studying the competition between alkyl-chain packing and π stacking in functionalized conjugated surfactants, the LB method in combination with structural studies has previously provided new guidelines for the design of molecules; these

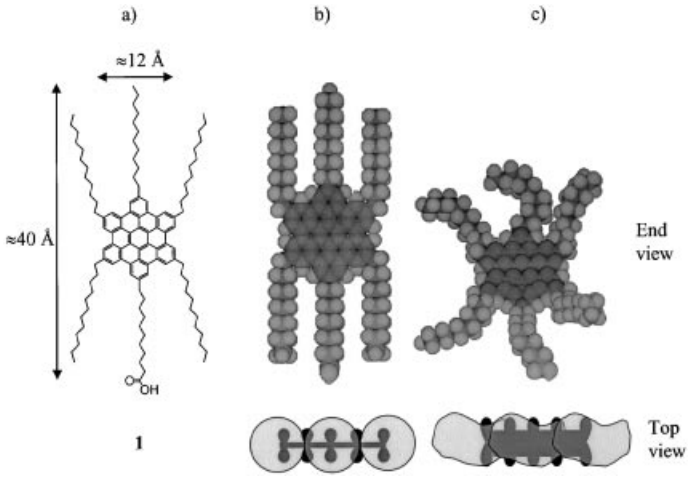

Figure 1. a) Molecular structure of the molecule studied, with approximate dimensions according to standard bond lengths and angles. b) Schematic end-view and top-view of the molecule that has crystalline alkyl chains. The top-view shows the alkyl chains as gray circles and the core π-conjugated system as a black line with protruding p orbitals. c) Schematic end-view and top-view of the molecule having disordered alkyl chains. The top-view representations in b) and c) is used throughout.

allow the frequently competing packing motives of alkyl chains and π stacks to co-exist without distorting the desired order in the π stack.[13–18] This competition of packing modes is also present in the HBC case in which the alkyl chains are connected to the periphery of a disk rather than to the edges of board-like molecules, as for example, polythiophenes.[14] We show here that, in this particular geometry, the packing competition gives rise to two distinct phases: one driven by π stacking, the other by alkyl-chain packing. As evidenced by diffraction and Kelvin force microscopy (KFM) studies presented below, this amphiphile self-assembles into lamellae on the water surface. In one phase, the π stacks are tilted in a similar manner to fallen domino bricks. In this case, the π stack is very well-ordered, as compared to bulk phases. We also demonstrate that this high degree of order leads to band formation in the one-dimensional columns. Application of lateral pressure forces the Langmuir film into another phase in which the alkyl chains are crystalline and coherence in the π stack is lost. This results in a measurable change in the electronic properties of the film. For these structural reasons it is expected that the charge-carrier mobility along the π stack will be exceptionally high in the low-pressure phase.

Results

Synthesis: The synthesis of the monoacid HBC-C_{12} (**1**) is outlined in Scheme 1.

Firstly, in a Hagihara–Sonoghashira coupling reaction, the monobromo-HBC (**2**) is treated with methyl undec-10-ynyloate to afford HBC derivative **3** in 80% yield. Reduction of **3** with a Pd/C catalyst in THF at room temperature gives **4** in 94% isolated yield. The final step of this sequence is the ester hydrolysis of **4**, which resulted in the acid-substituted HBC **1** in a yield of 80%. Details of the synthesis of **2** are given elsewhere.[19]

X-ray measurements: The compression isotherm of a Langmuir film of **1** is shown in Figure 2 (top). The crystal structure of the Langmuir film has been solved by grazing-incidence X-ray diffraction (GIXD)[20–22] at three different mean areas per molecule: 60 $Å^2$ molecule^{-1} (Figure 2 row 1), 80 $Å^2$ molecule^{-1} (Figure 2, row 2), and 100 $Å^2$ molecule^{-1} (Figure 2, row 3). The results show the coexistence of two different crystallographic phases. The high-pressure phase (Figure 2, row 1), measured at a mean area per molecule of 60 $Å^2$, shows three peaks at $2\theta_{xy}$ values of 5.47, 10.95, and 16.46° (Table 1). The peak with the highest angle ($2\theta_{xy} = 16.46°$) corresponds to a spacing of $d = 4.55$ Å. This peak resembles GIXD data from

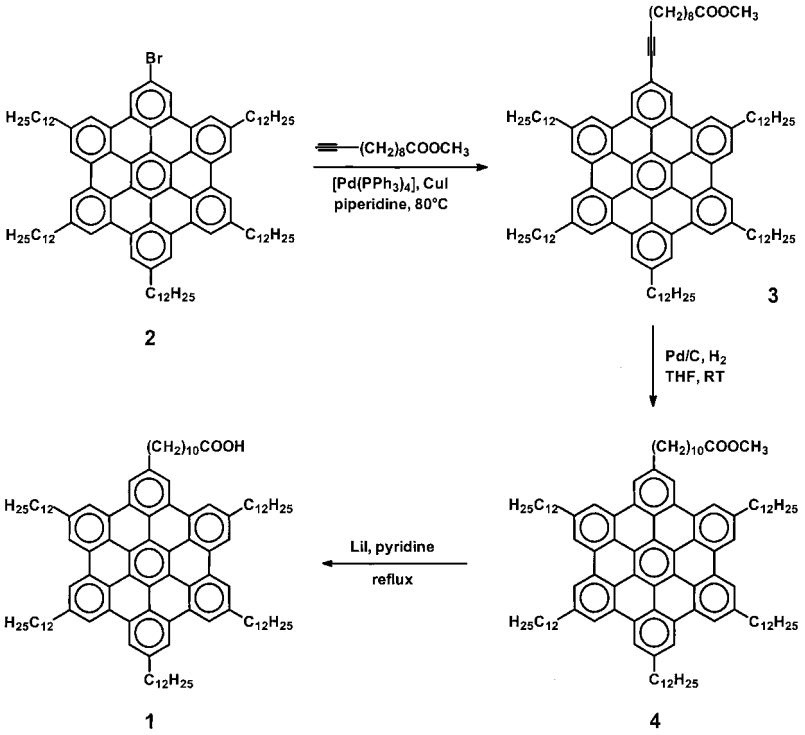

Scheme 1.

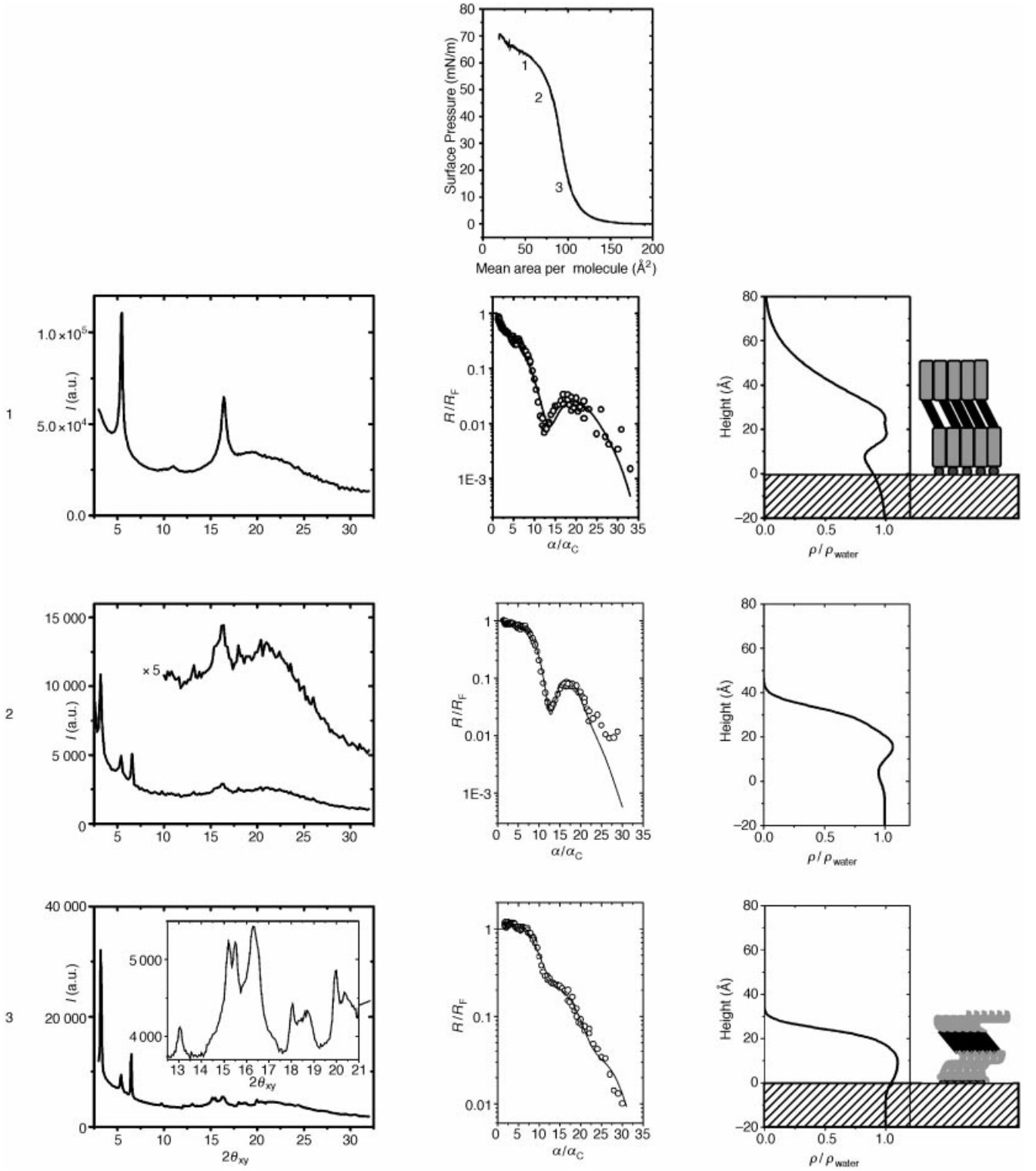

Figure 2. Top: Compression isotherm of HBC **1** at 21°C with numbers marking the monolayer states where X-ray measurements were performed. Left-hand column: The X-ray diffraction measured at different surface pressures (according to the numbers on the compression isotherm). The inset at the two lowest diffractograms is a magnification of the high angle regions. Middle column: The reflectivity data (○) and the result of fitting a three-slab model (——). Right-hand column: The electron-density profile arising from the three-step model, and the physical interpretation of the reflectivity data as a schematic drawing of the molecules in side-view on the water subphase (shaded box).

other amphiphiles with alkyl chains, for example, alcohols or carboxylic acids[20, 22] packed in a hexagonal lattice (if the structure was nonhexagonal, the peak would be split[20]). The two peaks at lower angles are believed to result from a trimerized superstructure of the alkyl chains linked to the HBC core. With six alkyl groups linked covalently to the HBC core, this would mean that three alkyl chains are pointing up from the HBC core and three are pointing down. The unit cell parameters of the high-pressure phase could not be uniquely determined, since no mixed-indexed {*hk*} reflections were

0947-6539/01/0722-4896 $ 17.50+.50/0 *Chem. Eur. J.* **2001**, *7*, No. 22

Table 1. Summary of GIXD data for the high-pressure phase.[a]

$2\theta_{xy}$ [°]	Q_{xy}[b]	d [Å][c]	Peak intensity	Index {hk}	Coherence length [Å][d]
5.47	0.46	13.66	strong	{10}	280
10.95	0.92	6.83	weak	{20}	150
16.46	1.38	4.55	strong	{01} (or {30})	120

[a] The tabulated values correspond to the X-ray diffractogram shown at the top of Figure 2 and measured at a mean area per molecule $A = 60$ Å^2. [b] Scattering vector. [c] Repeat distance. [d] The coherence lengths were calculated with the Scherrer formula.

observed; however, we propose the most likely structure to be hexagonal with the unit cell parameters $a = 3b = 15.78$ Å, $b = 5.26$ Å, $\gamma = 120°$, as shown in Figure 3b. This is in agreement with the atomic force microscopy (AFM) data shown below. The unit cell area is $A = 71.9$ Å^2, which indicates that the measurement taken at a mean molecular area of 60 Å^2 was performed after the collapse of the closely packed film.

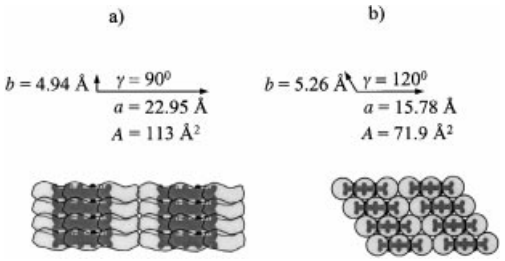

Figure 3. Structures of Langmuir films of amphiphilic HBC **1**. a) Above: unit cell parameters of the low-pressure phase with: $a = 22.95$ Å, $b = 4.94$ Å, and $\gamma = 90°$. Below: the schematic packing with the dark parts representing a top view of π-stacking conjugated parts of the molecules. b) Above: unit cell parameters of the high-pressure phase: $a = 3b = 15.78$ Å, $b = 5.26$ Å, $\gamma = 120°$, $A = 71.9$ Å^2. Below: the schematic packing with circles showing the hexagonal close-packed alkyl chains that are trimerized on account of their covalent linkage to the conjugated core of the molecule shown in black with protruding p orbitals. Compared to the low-pressure phase (a), the π overlap in the high-pressure phase (b) is diminished.

At a reduced surface pressure of 50 mN m^{-1}, which corresponds to a nominal area of 80 Å^2 per molecule, the coexistence of two phases is observed. At a further reduction in surface pressure to a nominal area per molecule of 100 Å^2, mainly diffraction from a low-pressure phase is seen. The diffraction from this low-pressure phase comes from a crystal structure with a uniquely identified rectangular unit cell: $a = 22.95$ Å, $b = 4.94$ Å, $\gamma = 90°$, $A = 113.4$ Å$^2 = 3 \times 37.8$ Å^2 (Figure 3a). All of the unusually high number of observed reflections can be indexed according to this unit cell (except two, marked with "hp" in Table 2, which result from a reminiscent high-pressure phase). The molecules form columnar stacks at the water surface, with an intercolumnar spacing along the a axis and with the repeat distance $b = 4.94$ Å along the stack. The HBC core is in a tilted orientation in the low-pressure phase (as evidenced by X-ray reflectivity, see below). This is in agreement with the notion that the normal π–π contact distance between the HBC cores is ≈3.5 Å,[4] which implies that the MAHBC core is tilted by ≈45° with respect to the surface normal to allow the projected

Table 2. Summary of GIXD data for the low-pressure phase.[a]

$2\theta_{xy}$ [°]	Q_{xy}[b]	d [Å][c]	Peak intensity	Index {hk}[d]	Coherence length[e] [Å]
3.26	0.27	22.95	very strong	{10}	323
5.4	0.45	13.8	medium	hp{10}	303
6.51	0.55	11.48	strong	{20}	462
9.78	0.82	7.66	very weak	{30}	253
13.05	1.10	5.74	weak	{40}	252
15.17	1.27	4.94	medium	{01}	175
15.51	1.30	4.83	medium	{11}	180
16.3	1.37	4.60	medium–strong	hp{01}/{50}	–
18.05	1.51	4.15	weak	{31}	284
20.0	1.68	3.74	medium–weak	{41}	208
22.4	1.87	3.36	very weak	{51}	259

[a] The tabulated values correspond to the X-ray diffractogram shown at the bottom of Figure 2 and measured at a mean area per molecule $A = 100$ Å^2. [b] Scattering vector. [c] Repeat distance. [d] The {hk} index corresponds to the unit cell parameters $a = 22.95$ Å, $b = 4.94$ Å, and $\gamma = 90°$, with the hp indices arising from high-pressure peaks coexisting with the low-pressure phase. [e] The coherence lengths were calculated from peak widths with the Scherrer formula.[38]

repeat distance of 4.94 Å. The coherence lengths along the stack are estimated from the peak-widths to be 200–400 Å (Table 2).

It is important to notice that the coherence of the conjugated π stack (as evidenced by the peaks at $2\theta_{xy}$ values between 15° and 23°) is lost in the transition from the low- to the high-pressure phase. This is most likely a consequence of the incommensurability between the crystal structure of the closely packed alkyl chains (being closely packed by the applied surface pressure) and the structure of the π stack. The loss of coherence in the π stack gives rise to a change in the electronic potential, as shown by Kelvin force microscopy (KFM) measurements on transferred films (see below).

It is not directly evident from the compression isotherm that two phases coexist, since no horizontal region in the compression isotherm is observed, as is typically found in lipid systems, for example.[23] The absence of such a horizontal region can be due to the high crystallinity (compared to lipids) of the monolayer resulting in very long equilibration times.

The vertical electron-density profile of the Langmuir monolayer has been determined by X-ray reflectivity measurements[20–22] performed at the same surface pressures as the diffraction experiments described above. The measured data are shown in Figure 2 (middle column, circles) along with the fit to the data (solid line). The reflectivity curves show that as the pressure is increased, the thickness of the monolayer increases as expected. The fit to the reflectivity data of the low-pressure phase gives a monolayer thickness of ≈30 Å. This thickness is so small that the molecules must be in a tilted conformation, since the length of the fully extended molecule is ≈40 Å (Figure 1). As the pressure is increased, the electron-rich conjugated center of the molecules is clearly seen as a protrusion of the electron-density curve, with the electron-poor alkyl layers below and above. The fit to the reflectivity data of the high-pressure phase shows a vertical tailing of the electron density (up to ≈80 Å). This indicates that a portion of the molecules is beginning to be pushed out of the monolayer (collapse).

The reflectivity fits are in agreement with the model described above: at low pressure the molecules are tilted and efficient and coherent packing is obtained, which is dominated by π stacking. This coherence is then lost on compression.

Scanning probe microscopy (SPM) measurements on films transferred to solid supports: Deflection-mode atomic force microscopy (AFM) can be used to obtain images of the high-pressure phase with atomic resolution. Figure 4 shows data for an LB monolayer transferred onto mica by horizontal lifting from a Langmuir film compressed to $A = 80$ Å^2 (transferred by having the substrate in the aqueous subphase prior to spreading of the monolayer).[24] Images of the high-pressure phase with atomic resolution show that it consists of closely packed (crystalline) alkyl chains that protrude from the surface. The repeat distances are $a = 5.1$ Å and $b = 4.5$ Å, while $\gamma = 108°$. The area of the unit cell is $A_{AFM} = 21.8$ Å^2. One possible orientation of the molecules as seen from the top is sketched in. The deviation from the observed X-ray data ($a = 3b = 15.78$ Å (trimerized), $b = 5.26$ Å, $\gamma = 120°$, $A = 71.9$ Å$^2 = 3 \times 23.9$ Å^2) could be the result of relaxation during transfer to a solid support, [18] although it is more likely to be a consequence of nonlinearity in the AFM piezoes.

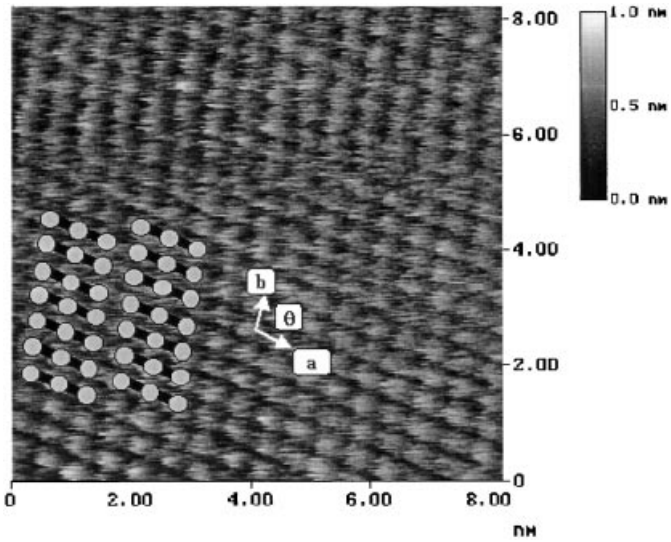

Figure 4. Contact (deflection)-mode AFM image of an LB monolayer of HBC **1** transferred from the air–water interface to atomically flat mica at a mean area per molecule $A = 80$ Å^2 (high-pressure phase). The cell parameters drawn are $a = 5.1$ Å, $b = 4.5$ Å, and $\gamma = 108°$. A cartoon of HBC molecules stacked along a horizontal direction is shown, in which each molecule has three protruding alkyl chains.

Kelvin force microscopy (KFM): Figure 5 shows a tapping-mode AFM micrograph of the topography of a monolayer of HBC as well as a Kelvin force microscopy (KFM)[25] image showing the electrical potential of the same monolayer film of **1** transferred to a solid support (a Si wafer with a natural hydrophilic oxide coating) by horizontal lifting from a HBC-monolayer compressed to a mean molecular area $A = 100$ Å^2. This area corresponds to a point in the phase diagram that is

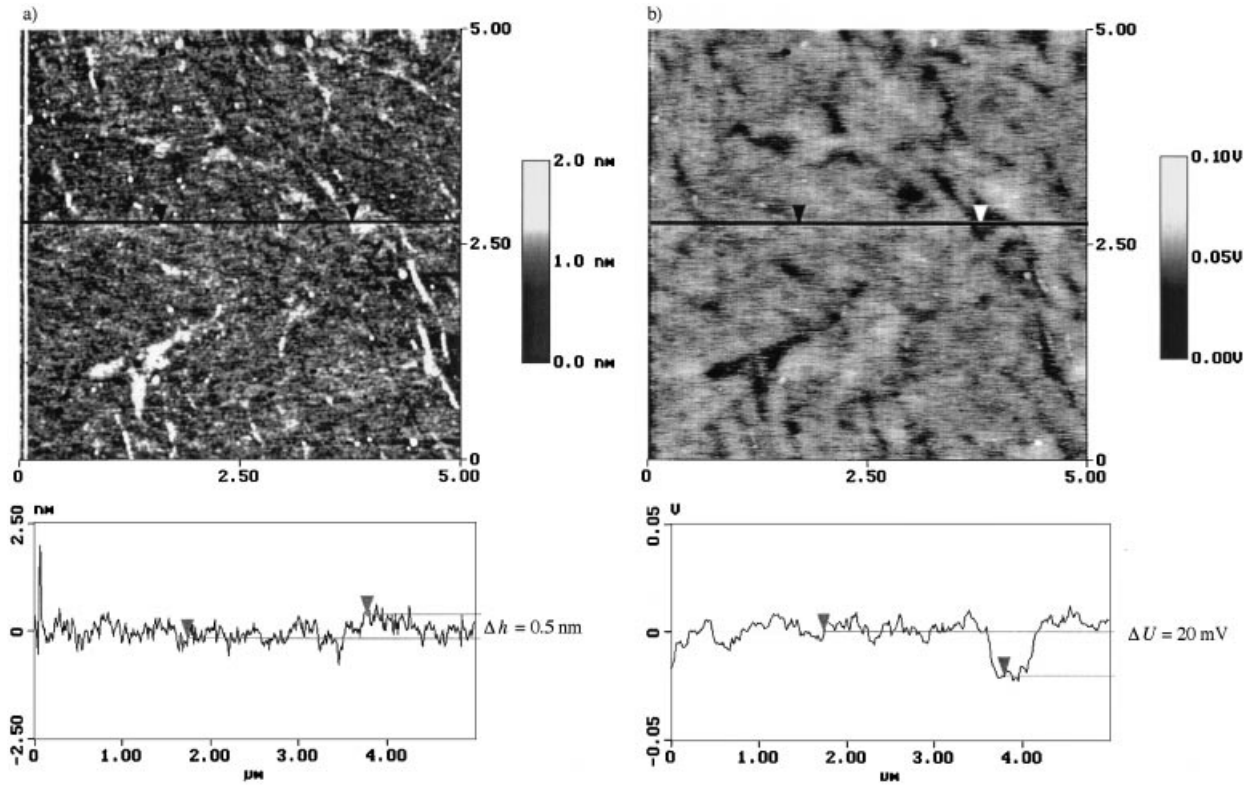

Figure 5. a) AFM tapping-mode topography image of a LB monolayer of HBC **1** transferred to a Si wafer with a natural oxide layer at a mean area per molecule $A = 100$ Å^2. Also shown is a cross-section profile from the middle of the scan, showing the height difference between the high-pressure and the low-pressure phases. The height difference is ≈5 Å. b) KFM image showing the potential landscape of the same area as that shown in a). The potential of the low-pressure phase is ≈20 mV higher than the potential of the high-pressure phase, as also can be seen from the cross-section profile.

0947-6539/01/0722-4898 $ 17.50+.50/0 *Chem. Eur. J.* **2001**, *7*, No. 22

dominated by the low-pressure phase (Figure 2, row 3). The presence of two phases is clearly visible as height differences in the topography image shown in Figure 5a. The height difference between the two phases is of the order of 5 Å, which agrees with the height differences seen in the reflectivity data (see Figure 2). The height difference suggests that the high areas are domains of molecules in the high-pressure phase, with surroundings that consist of molecules in the low-pressure phase. This is also supported by the fact that the alkyl packing seen by AFM in Figure 4 could only be found in the high areas. The KFM micrograph (Figure 5b) shows that the surface potential is inversely correlated to the topography graph: the domains which are high in topography have low potential and vice versa. The measured nominal potential difference of 20 meV is in the range generally observed for bandwidths of π stacks.[26]

Discussion and Conclusions

A prerequisite of high charge-carrier mobility in thin films of discotic molecules is coherent order in the π stack. To allow for processability from solutions, the molecules must also be soluble, in which case the molecules are disordered in solution. Hexaalkylated hexa-*peri*-hexabenzocoronene with solubilizing alkyl substituents has proven a good candidate for balancing these often counteracting requirements and indeed, high mobilities have been measured for bulk alkyl- and phenylenealkyl-substituted HBC.[8] In order to investigate the HBC system further, we have synthesized and characterized an HBC molecule in which one of the alkyl chains is terminated by a carboxylic acid group. For the amphiphilic structure **1**, high coherence is observed for the self-assembled Langmuir films at the air–water interface, as evidenced by X-ray diffraction: in our investigation of the Langmuir films we found an unprecedented large number of sharp reflections in the X-ray diffractograms that arise from a highly coherent π stack (coherence lengths of 200–400 Å). Thus, preparation by means of Langmuir films seems to be a promising route to highly ordered thin films with good charge-carrier mobilities.

For practical applications, the thin films need to be transferred to solid supports. Here the films were transferred by horizontal lifting and were examined by AFM and KFM. It was shown that coexistence of the two phases persisted during transfer and that the two phases have different electronic properties. The KFM experiment can be explained on the basis of a PN junction, which has a built-in potential drop across the junction which will have a negative P side and a positive N side because electrons flow from the N side to the P side to recombine with the holes on the P side. The potential of the N side will therefore rise above the P side in the KFM image, as described in various papers.[27–32] On the basis of our structural data, we assume that the HBC electrons are delocalized along the π stack in the low-pressure areas, and, hence, we expect the formation of a band structure that gives rise to a reduction in the HOMO–LUMO gap relative to the localized HBC core (Figure 6a). In the high-pressure domains, we assume that the electrons are highly localized on the molecules. These assumptions are supported by our X-ray data, which indicate that coherence between the graphite disks exists in the low-pressure phase, leading to a better π–π overlap than in the high-pressure phase (see Figure 2), in which the coherence in the π stack is lost. When the two phases are brought into contact, the more loosely bound electrons lying high in the "conduction" band of the low-pressure phase will be attracted to the more tightly bound molecular orbitals in the high-pressure phase. As a result a small amount of electrons (<10)[33] will be transferred from the low- to high-pressure domains. This will leave the low-pressure areas slightly positive and the high-pressure domains slightly negative;[34] this is also observed in the KFM micrograph in Figure 5. This representation is compatible with the representation of the PN junction presented above, in which the low-pressure phase corresponds to the N side and the high-pressure phase to the P side.

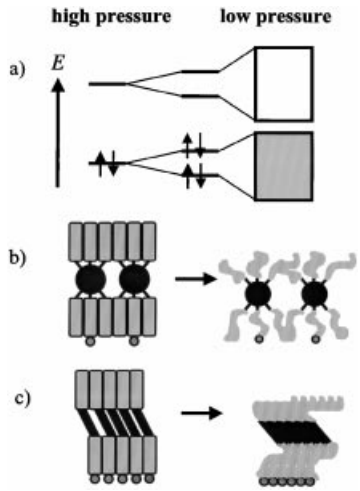

Figure 6. Schematic drawing of the transformation from the high- to low-pressure phase. a) The electronic structure changes caused by delocalization of the localized HBC states as the pressure is decreased. b) View along the lamellae (end view). The alkyl chains are closely packed in the high-pressure phase and disordered in the low-pressure phase. c) Side view of a lamella of the high-pressure phase (left) and low-pressure phase (right). In the low-pressure phase a close π–π contact is obtained.

The absolute value of the potential difference between the two phases is difficult to access, since a correction of the data is needed. This is a consequence of the fact that the electrical forces are long range, and as a consequence the potential seen by the KFM probe is actually a sum of many contributions, with the area underneath the probe as the leading term.[35–37] Nevertheless, we note that the measured potential difference between the high- and low-pressure phases is in good agreement with typical values of the bandwidth in π stacks.[26]

Our results are summarized schematically in Figure 6. It illustrates the anticipated packing motifs of the molecules seen along the lamellae (b) together with a side view (c) which represents the coherent π stacks in the low-pressure phase (right-hand side) and the closely packed alkyl chains (with a larger π–π distance) in the high-pressure phase (left-hand side). Figure 6a illustrates the band formation as indicated by the KFM measurements; the domains which have a high topography (the high-pressure phase) have localized states, whereas a more delocalized structure is seen in the low-pressure phase.

Experimental Section

2-(10-Methoxycarbonylundec-1-inyl)-5,8,11,14,17-pentadodecylhexa-*peri*-hexabenzocoronene (3): 2-Bromo-5,8,11,14,17-pentadodecylhexa-*peri*-hexabenzocoronene (**2**, 1.0 g, 0.69 mmol), copper(I) iodide (572 mg, 0.30 mmol) and $[Pd^0(PPh_3)_4]$ (182 mg, 0.157 mmol) were dissolved in piperidine (200 mL) under an argon atmosphere. After addition of methyl undec-10-ynyloate the reaction was stirred at 80 °C for 24 hours. This solution was then poured into a saturated NH_4Cl solution and extracted with hot toluene several times. The combined organic layers were then washed with saturated NH_4Cl solution and water. Drying with $MgSO_4$ and evaporation of the solvent under vacuum followed by column chromatography (silica, CH_2Cl_2/toluene) yielded **3** (868 mg, 80 %) as yellow crystals. ^{1}H NMR (500 MHz, $CDCl_3/CS_2$ 1:1): $\delta = 8.40$ (s, 2H; Ar*H*), 8.13 (s, 2H; Ar*H*), 8.02 (s, 4H; Ar*H*), 7.99 (s, 2H; Ar*H*), 7.98 (s, 2H; Ar*H*), 3.67 (s, 3H; OCH_3), 2.89 (t, $^3J = 7.9$ Hz, 2H; ArCH_2), 2.87 (t, $^3J = 7.9$ Hz, 4H; ArCH_2), 2.83 (t, $^3J = 8.1$ Hz, 4H; ArCH_2), 2.78 (t, $^3J = 7.3$ Hz, 2H; ≡CCH_2), 2.38 (t, $^3J = 7.5$ Hz, 2H; OCCH_2), 2.03 – 1.80 (m, 12H; CH_2), 1.80 – 1.72 (m, 4H; CH_2), 1.67 – 1.25 (m, 96H; CH_2), 0.90 (t, $^3J = 9.6$ Hz, 15H; CH_3); ^{13}C NMR (125 MHz, $CDCl_3/CS_2$ 1:1): $\delta = 173.44$ (*C*=O), 139.29, 139.13, 139.10, 129.83, 129.02, 128.96, 128.81, 128.45, 123.60, 123.21, 122.48, 122.29, 120.92, 120.65, 120.53, 120.45, 119.08, 118.94, 118.68, 118.17, 89.82 (C_{ar}-*C*≡), 82.48 (≡*C*CH$_2$), 51.06 (O*C*H$_3$), 37.29, 37.20, 34.02, 32.45, 32.39, 32.05, 31.98, 30.31, 30.27, 30.10, 30.04, 29.96, 29.88, 29.54, 29.45, 29.41, 25.09, 22.88, 20.15, 14.19 (*C*H$_3$); FD-MS calcd: *m*/*z* (%): 1557.23 (100) $[M]^+$; found: 1558.2; IR: $\tilde{\nu} = 3062$, 2951, 2919, 2850, 1743 (C=O), 1611, 1466, 861 cm^{-1}; UV/Vis: λ (log ε) = 330 (4.45), 346 (4.86), 363 (5.22), 374 (4.80), 394 (4.73), 407 nm (4.27); elemental analysis calcd (%) for $C_{114}H_{156}O_2$: C87.86, H10.09; found: C87.78, H10.14.

2-(10-Methoxycarbonylundecyl)-5,8,11,14,17-pentadodecylhexa-*peri*-hexabenzocoronene (4): Compound **3** (893 mg, 0.53 mmol) was dissolved in THF (200 mL) and Pd/C (10 %, 285 mg) was added. The mixture was hydrogenated with H_2 (1 bar) at room temperature for 16 hours. The catalyst was filtered off, and the solvent was removed under reduced pressure. The remaining solid was purified by column chromatography (silica, CH_2Cl_2/toluene) followed by recrystallisation from *n*-heptane to afford **4** (786 mg, 94 %) as yellow crystals. ^{1}H NMR: (500 MHz, $CDCl_3/CS_2$ 1:1): $\delta = 8.26 – 8.20$ (br, 12H; Ar*H*), 3.62 (s, 3H; OCH_3), 2.93 (br, 12H; ArCH_2), 2.28 (t, $^3J = 7.5$Hz, 2H; OCCH_2), 1.92 (br, 12H; ArCH$_2$CH_2), 1.66 – 1.23 (m, 104H; CH_2), 0.89 (m, 15H; CH_3); ^{13}C NMR (125 MHz, $CDCl_3/CS_2$ 1:1): $\delta = 173.53$ (C=O) (low intensity), 139.42, 129.36, 122.91, 120.78, 119.15, 51.05 (O*C*H$_3$), 37.29, 33.99, 32.51, 32.37, 32.04, 30.21, 30.05, 30.01, 29.93, 29.85, 29.76, 29.53, 29.48, 29.31, 25.02, 22.86, 14.18 (*C*H$_3$); FD-MS calcd: *m*/*z* (%):1561.24 (100) $[M]^+$; found 1561.6; IR: $\tilde{\nu} = 3062$, 2951, 2919, 2850, 1744 (C=O), 1611, 1467, 860 cm^{-1}; UV/Vis: λ (log ε) = 327 (4.50), 344 (4.94), 360 (5.30), 371 (4.91), 391 (4.83), 404 nm (4.29); elemental analysis calcd (%) for $C_{114}H_{160}O_2$: C87.83, H10.32; found: C87.65, H10.35.

2-(10-Carboxy-undecyl)-5,8,11,14,17-pentadodecylhexa-*peri*-hexabenzocoronene (1): Compound **4** (396 mg, 0.253 mmol) and LiI (3.77 g, 28.16 mmol) were suspended in pyridine (40 mL) under an argon atmosphere. The resulting mixture was heated under reflux for 12 hours. After removing the solvent, water was added to the mixture which was then acidified with 10 % HCl solution. The crude product was extracted several times with hot toluene. The solvent of the combined organic layers was removed under reduced pressure, and the resulting solid was recrystallized from *n*-heptane to yield 313 mg (80 %) of **1** as yellow crystals. ^{1}H NMR (500 MHz, $CDCl_3/CS_2$ 1:1): $\delta = 8.01$ (br, 12H; Ar*H*), 2.79 (br, 12H; ArCH_2), 2.39 (br, 2H; OCCH_2), 1.86 (br, 12H; ArCH$_2$CH_2), 1.74 – 1.23 (m, 104H; CH_2), 0.89 (t, $^3J = 6.0$ Hz, 15H; CH_3); ^{13}C NMR (125 MHz, $CDCl_3/CS_2$ 1:1): $\delta = 139.01$, 129.06, 122.62, 120.44, 118.81, 37.21, 32.52, 32.05, 30.27, 30.08, 30.03, 29.95, 29.87, 29.53, 22.86, 14.17 (*C*H$_3$); FD-MS calcd: *m*/*z* (%): 1547.22 (100) $[M]^+$; found 1548.9; IR: $\tilde{\nu} = 3062$, 2951, 2920, 2850, 1709 (C=O), 1611, 860 cm^{-1}; UV/Vis: λ (log ε) = 314 (4.07), 327 (4.27), 344 (4.68), 360 (5.03), 371 (4.69), 383 (4.53), 391 (4.60), 403 (4.13), 415 nm (3.87).

Langmuir and Langmuir – Blodgett films, and X-ray measurements: Monolayers of the amphiphilic HBC derivative **1** were easily spread from chloroform solutions (≈0.5 mg mL^{-1}) onto the neutral Milli-Q purified water subphase (18.2 MΩ cm) in an LB trough. The subphase was thermostated to 21 °C. Because of the high crystallinity of the Langmuir film, transfer to solid supports by the standard Langmuir – Blodgett technique with vertical dipping was not applicable; however, transfer was possible by horizontal lifting[24] (the substrate was placed below the water subphase prior to the spreading, and transferred at 0.1 mm min^{-1}). The substrates used for the LB films for KFM measurements were highly doped Si-wafers with natural oxide layers. The X-ray measurements were performed at the X-ray undulator beamline BW1 at the synchrotron facility HASYLAB at DESY in Hamburg (Germany). The X-ray wavelength was $\lambda = 1.304$ Å, monochromated by the Bragg reflection from a Be(002) crystal. Two different X-ray techniques were used:[20–22] grazing-incidence X-ray diffraction (GIXD) and specular reflectivity (XR). For the GIXD, the grazing angle of incidence (α_i) was slightly below the critical angle (α_c) for total reflection ($\alpha_i = 0.85\,\alpha_c$) thus increasing the surface sensitivity by minimizing the penetration depth of the incident X-rays into the water subphase. The horizontal scattering angle ($2\theta_{xy}$) was resolved with a Soller collimator. The XR experiments probed the vertical electron-density profile across the interface by varying the incident angle (α_i) and the exit angle ($\alpha_f = \alpha_i$) simultaneously, and the intensity pattern that results from interference between rays reflected at different depths was recorded. The experimental data are shown as the measured reflectivity (R) normalized to the Fresnel reflectivity (R_F) from a theoretically sharp water surface as a function of α_i/α_c. The data were fitted by a previously described method[20, 21] by means of a model with three slabs of (different) constant electron densities stacked on the water subphase. To account for thermally generated capillary waves on the water surface, the electron density of these slabs was smeared by convolution with a gaussian. The resulting smeared electron-density profiles are shown in Figure 2.

Atomic force microscopy (AFM) and Kelvin force microscopy (KFM): These were performed with a Nanoscope III from Digital Instruments. The AFM measurements with atomic resolution were performed with standard silicon nitride tips in the deflection mode. For the KFM measurements, a metal-coated tapping-mode tip was mounted into a holder that allowed electrical connection to the tip itself. When scanning the surface of a substrate, the so-called lift mode was engaged; thus two scans were made in each cycle. The first scan recorded the surface profile. In the second scan, the tip tracked the surface at a fixed distance without tapping, but with an applied AC field that was tuned to the resonant frequency of the cantilever. If the tip encountered any electrostatic force that was different from the ground, it started vibrating. By the use of a feedback loop, the force on the tip was nullified by the application of a DC potential to the tip to counteract the potential on the surface.

Acknowledgements

We thank the Danish Research Councils (SNF, STVF, MUP, grants 9400892, 9501197, DanSync), the European Community (IHP Contract HPRI-CT-1999 – 00040), the Volkswagenstiftung, and the European Commission (TMR program SISITOMAS) for support and HASYLAB at DESY, Hamburg (Germany) for beamtime at beamline BW1.

[1] *J. Mater. Chem.* **1999**, *9*, Special issue on Functionalized Organic Materials for Devices.
[2] N. Boden, R. J. Bushby, J. Clements, B. Movaghar, *J. Mater. Chem.* **1999**, *9*, 2081.
[3] A. M. van de Craats, J. M. Warman, K. Müllen, Y. Geerts, J. D. Brand, *Adv. Mater.* **1998**, *10*, 36.
[4] P. Herwig, C. W. Kayser, K. Müllen, H. W. Spiess, *Adv. Mater.* **1996**, *8*, 510.
[5] V. S. Iyer, K. Yoshimura, V. Enkelmann, R. Epsch, J. P. Rabe, K. Müllen, *Angew. Chem.* **1998**, *110*, 2843; *Angew. Chem. Int. Ed.* **1998**, *37*, 2696.
[6] M. Müller, C. Kubel, K. Müllen, *Chem. Eur. J.* **1998**, *4*, 2099.
[7] F. Morgenroth, A. J. Berresheim, M. Wagner, K. Müllen, *Chem. Commun.* **1998**, 1139.
[8] A. M. van de Craats, J. M. Warman, A. Fechtenkotter, J. D. Brand, M. A. Harbison, K. Müllen, *Adv. Mater.* **1999**, *11*, 1469.
[9] A. F. Thunemann, D. Ruppelt, C. Burger, K. Müllen, *J. Mater. Chem.* **2000**, *10*, 1325.

[10] A. F. Thuneman, D. Ruppelt, S. Ito, K. Müllen, *J. Mater. Chem*. **1999**, *9*, 1055.
[11] I. Langmuir, *J. Am. Chem. Soc*. **1917**, *39*, 1848.
[12] K. B. Blodgett, *J. Am. Chem. Soc*. **1935**, *57*, 1007.
[13] P. Delhaès, V. M. Yartsev, *Electronic and Spectroscopic Properties of Conducting Langmuir–Blodgett Films* (Eds: R. J. H. Clark, R. E. Hester), Wiley, **1993**, pp. 199–289.
[14] N. Reitzel, D. R. Greve, K. Kjaer, P. B. Howes, M. Jayaraman, S. Savoy, R. D. McCullough, J. T. McDevitt, T. Bjørnholm, *J. Am. Chem. Soc*. **2000**, *122*, 5788.
[15] T. Bjørnholm, T. Hassenkam, N. Reitzel, *J. Mater. Chem*. **1999**, *9*, 1975.
[16] M. R. Bryce, M. C. Petty, *Nature* **1995**, *374*, 771.
[17] M. Vandevyver, *J. Chim. Phys. Phys.-Chim. Biol.* **1988**, *85*, 1033.
[18] J. Garnaes, N. B. Larsen, T. Bjørnholm, M. Jørgensen, K. Kjaer, J. Als-Nielsen, J. F. Jørgensen, J. A. Zasadzinski, *Science* **1994**, *264*, 1301.
[19] S. Ito, M. Wehmeier, J. D. Brand, C. Kübel, R. Epsch, J. P. Rabe, K. Müllen, *Chem. Eur. J.* **2000**, *6*, 4327.
[20] J. Als-Nielsen, D. Jacquemain, K. Kjaer, F. Leveiller, M. Lahav, L. Leiserowitz, *Phys. Rep*. **1994**, *246*, 251.
[21] J. Als-Nielsen, H. Möhwald in *Handbook on Synchrotron Radiation, Vol. 4* **1991**, p. 3.
[22] K. Kjaer, *Physica B* **1994**, *198*, 100.
[23] *Langmuir–Blodgett Films* (Ed.: G. Roberts), Plenum, New York **1990**.
[24] I. Langmuir, V. J. Schaefer, *J. Am. Chem. Soc*. **1938**, *60*, 1351.
[25] M. Nonnenmacher, M. P. O'Boyle, H. K. Wickramasinghe, *Appl. Phys. Lett*. **1991**, *58*, 2921.
[26] A. J. Berlinsky, J. F. Carolan, *Solid State Commun*. **1974**, *15*, 795.
[27] A. K. Henning, T. Hochwitz, J. Slinkman, J. Never, S. Hoffmann, P. Kaszuba, C. Daghlian, *J. Appl. Phys.* **1995**, *77*, 1888.
[28] A. Kikukawa, S. Hosaka, R. Imura, *Appl. Phys. Lett*. **1995**, *66*, 3510.
[29] A. Chavezpirson, O. Vatel, M. Tanimoto, H. Ando, H. Iwamura, H. Kanbe, *Appl. Phys. Lett*. **1995**, *67*, 3069.
[30] T. Mizutani, T. Usunami, S. Kishimoto, K. Maezawa, *Jpn. J. Appl. Phys. Part 1* **1999**, *38*, 4893.
[31] T. Mizutani, T. Usunami, S. Kishimoto, K. Maezawa, *Jpn. J. Appl. Phys. Part 2* **1999**, *38*, L767.
[32] T. Meoded, R. Shikler, N. Fried, Y. Rosenwaks, *Appl. Phys. Lett*. **1999**, *75*, 2435.
[33] An estimate of the number of carriers can be given by examining the almost circular high-pressure domain seen under the leftmost marker in the KFM image (Figure 5). Assuming that this domain and its immediate surroundings can be modeled as two coaxial cylinders with a radius of $b = 220$ nm and $a = 219.5$ nm, the capacitance is given by Equation (1):

$$C = \frac{2\pi\varepsilon t}{\ln b/a} \quad (1)$$

in which t is the thickness of the monolayer and ε is the dielectric constant. The number of charges on the inner domain can then be found from the basic equation of capacitance [Eq. (2)]:

$$Q = CV \quad (2)$$

For a vacuum dielectric constant of $\varepsilon = 8.85 \times 10^{-12}\ \mathrm{Fm}^{-1}$, a thickness $t \approx 3$ nm, and a voltage drop of $V = 20$ mV, the number of charges is calculated as given in Equation (3):

$$Q = \frac{2\pi \times 3 \times 10^{-9} \times 8.85 \times 10^{-12} \times 20 \times 10^{-3}}{\ln(220/219.5) \times 1.6 \times 10^{-19}} = 9 \quad (3)$$

This calculation of the order of magnitude indicates that the number of electrons is very low. The number of molecules inside the domain is about 212 000. Despite the fact that the film is undoped, the nine holes in the high-pressure phase to be filled by the nine electrons from the low-pressure phase can easily be explained by impurities, corrupted molecules etc.
[34] H. O. Jacobs, A. Stemmer, *Surf. Interface Anal*. **1999**, *27*, 361.
[35] H. O. Jacobs, H. F. Knapp, A. Stemmer, *Rev. Sci. Inst*. **1999**, *70*, 1756.
[36] H. O. Jacobs, P. Leuchtmann, O. J. Homan, A. Stemmer, *J. Appl. Phys.* **1998**, *84*, 1168.
[37] H. O. Jacobs, H. F. Knapp, S. Muller, A. Stemmer, *Ultramicroscopy* **1997**, *69*, 39.
[38] A. Guinier, *X-ray Diffraction*, Freeman, San Francisco **1963**.

Received: January 29, 2001
Revised: June 18, 2001 [F3031]